

***In situ* nuclear magnetic resonance investigation of deformation-generated vacancies in aluminum**

K. Detemple and O. Kanert

Institute of Physics, University of Dortmund, 44221 Dortmund, Germany

J. Th. M. De Hosson

Department of Applied Physics, University of Groningen, 9747 AG Groningen, The Netherlands

K. L. Murty

North Carolina State University, Raleigh, North Carolina 27695-7909

(Received 1 December 1994)

Enhanced atomic diffusion under plastic deformation was observed in aluminum by means of an improved rotating-frame nuclear-spin-relaxation technique. The enhancement is caused by excess vacancies formed by the deformation process. ^{27}Al NMR experiments were carried out as a function of temperature on polycrystalline, pure aluminum foils during deformation at constant strain rates. Evaluation of the data yields the actual concentration of the excess vacancies as a function of temperature, strain, and strain rate. The findings are in accord with a model which describes the formation mechanism of the vacancies through a fraction of the applied deformation power density (applied stress times strain rate) and the annihilation process by the diffusion of the vacancies to dislocations acting as vacancy sinks.

I. INTRODUCTION

There exists a large number of studies on the dynamics of point defects in metals introduced by plastic deformation. The experiments, however, were performed on materials cold-worked at various temperatures. Subsequent annealing of the specimens permits the measurement of recovery stages due to the kinetics of the different defects created by the deformation process. The recovery is mostly monitored by electrical resistivity;^{1,2} a large variety of other techniques, such as positron trapping,^{3,4} perturbed-angular correlation,⁵ ultrasonic attenuation,⁶ Mössbauer spectroscopy,⁷ and electron paramagnetic resonance⁸ are also applied to observe the recovery stages.

In contrast to these "two-step experiments," however, where the deformation process is separated from the observation of the defect kinetics, very few experiments were performed in the past measuring *in situ* the dynamics of deformation-induced defects during plastic deformation. Evidence of the formation of point defects by plastic deformation was provided by the observation of Gyulai and Hartly that plastic deformation causes an increase in the ionic conductivity of alkali halides.⁹ The experiments were repeated in more detail by Ueta and Känzig.¹⁰ Experimental investigations clearly indicate that also in metals atomic diffusion is enhanced during deformation due to the formation of point defects.^{11,12}

Generally, as the deformation process is very limited in time, in particular at high strain rates $\dot{\epsilon}$, one has to apply a fast and nondestructive experimental technique in order to measure *in situ* in actual state of the sample under deformation: Supposing a permissible variation $\Delta\epsilon \leq 1\%$ of the strain the experiment has to be performed in a time

interval $\Delta t \leq 0.01/\dot{\epsilon}$. As we have shown earlier¹³ nuclear magnetic resonance is one of the very few techniques which is able to observe *in situ* the dynamic properties of deformation-generated defects in sufficiently short times. For that, one has to measure the contribution to the nuclear-spin-relaxation (NSR) rate in the rotating frame, $1/T_{1\rho}$, which is induced by the dynamics of the defects under investigation. The actual relaxation rate is obtained from the time evolution of the nuclear magnetization in the rotating frame. Here, we present an improved $T_{1\rho}$ pulse sequence described in detail in Sec. III (CUT sequence) which allows us to measure precisely the complete magnetization decay in a "single-shot" which is of prime significance in a fast and correct determination of the relaxation rate of the deforming sample.

The sequence is applied to the study of strain-induced excess vacancies in pure aluminum. Aluminum is chosen since the concentration of thermal vacancies is very well known by results of positron annihilation experiments.⁴ Moreover, ^{27}Al is a suitable probe nucleus for the NSR experiments because of the large abundance (100%) and of a reasonable value of the gyromagnetic ratio. Unfortunately, the signal distortions problems related to the skin effect in metallic systems limits the study to thin foils which makes it relatively difficult to perform NMR experiments under deformation.

II. DIFFUSION-INDUCED NUCLEAR-SPIN RELAXATION

In metals such as aluminum atomic diffusion occurs by a monovacancy mechanism, i.e., the atomic jump rate Γ

is controlled by the concentration c_v of the monovacancies according to^{14,15}

$$\Gamma = \frac{1}{\tau} = c_v \Gamma_v . \quad (1)$$

Here, Γ_v denotes the jump rate of vacancies which is determined by a thermally activated process

$$\Gamma_v = \Gamma_0 \exp(-H_m/kT) , \quad (2)$$

where H_m is the migration enthalpy and Γ_0 is the attempt frequency of the process. In crystals with cubic symmetry the uncorrelated diffusion coefficient D is related to the jump rate Γ by

$$D = \frac{a_0^2}{6} \Gamma \quad (3)$$

with a_0 being the atomic jump distance. The coefficient D can be measured by transport experiments (radio tracer, ionic conductivity, etc.) taking into account the corresponding correlation factor of the actual diffusion mechanism.¹⁵ In pure metals the vacancies are of intrinsic nature, i.e., they are thermally created according to the relation

$$c_v = \exp(S_f/k) \exp(-H_f/kT) , \quad (4)$$

where S_f and H_f denote the entropy and enthalpy, respectively, for monovacancy formation.

An additional number of vacancies can be formed by various effects such as quenching, irradiation, or plastic deformation. These excess vacancies with concentration c_v^{ex} cause an increase of the atomic jump rate Γ according to Eq. (1). Supposing that the jump rate Γ_v of the vacancies remains unaltered as in the undeformed case, Eq. (1) can be extended as follows:

$$\Gamma = (c_v + c_v^{\text{ex}}) \Gamma_v = c_v^{\text{total}} \Gamma_v . \quad (5)$$

The atomic jumps induce fluctuations of nuclear-spin interactions giving rise to a nuclear-spin-lattice relaxation process. The strength of the relaxation process is described by the nuclear-spin-relaxation rate, which is related under rotating frame conditions to the atomic jump rate Γ as follows:¹⁶

$$\frac{1}{T_{1\rho}} \Big|_{\text{Diff}} = A(\omega_1) \frac{\langle \omega_\rho^2 \rangle}{2\omega_{\text{eff}}} J(\omega_{\text{eff}}/\Gamma) \quad (6)$$

with

$$A(\omega_1) = \frac{\omega_1^2 + \delta \omega_{\text{loc}}^2}{\omega_{\text{eff}}^2} . \quad (6a)$$

Here, $\langle \omega_\rho^2 \rangle$ denotes the mean-square spin interaction responsible for the relaxation process, ω_{loc}^2 is the mean-square local field consisting of a dipolar and a strain-dependent quadrupolar contribution, i.e., $\omega_{\text{loc}}^2 = \omega_D^2 + \omega_Q^2(\epsilon)$, $\omega_{\text{eff}} = (\omega_1^2 + \omega_{\text{loc}}^2)^{1/2}$ is the effective Larmor frequency in the rotating frame with $\omega_1 = \gamma B_1$ being the external frequency due to the locking field B_1 (γ is the gyromagnetic ratio of the spins), and $J(x)$ is the spectral density of the pair-correlation function $G(t)$ of the

diffusing atoms.^{15,17} The coefficient $A(\omega_1)$ varies between the factor δ and one depending on the strength of ω_1 , where δ is of the order of two.¹⁷

In the present investigation we have used the Torrey approach¹⁸ for evaluating the experimental data, i.e., $J(x) = J_{\text{Torrey}}(x)$ in Eq. (6). Further, as shown by the experiments (see Sec. IV) deformation-induced contributions to $1/T_{1\rho}|_{\text{Diff}}$ were observed only at the low-temperature site of the maximum of $1/T_{1\rho}|_{\text{Diff}}$ which occurs for $\omega_{\text{eff}} = \Gamma$, i.e., the condition $\Gamma < \omega_{\text{eff}}$ is fulfilled for all the experiments dealing with the properties of the excess vacancies. Then, Eq. (6) can be written as follows:¹⁶

$$\frac{1}{T_{1\rho}} \Big|_{\text{Diff}} = A(\omega_1) \frac{\langle \omega_\rho^2 \rangle}{4\omega_{\text{eff}}^2} \Gamma \quad (7)$$

or, using Eq. (5)

$$\begin{aligned} \frac{1}{T_{1\rho}} \Big|_{\text{Diff}} &= \frac{1}{T_{1\rho}} \Big|_{\text{Diff}}^0 + \frac{1}{T_{1\rho}} \Big|_{\text{Diff}}^{\text{ex}} \\ &= A(\omega_1) b_\rho c_v + A(\omega_1) b_\rho c_v^{\text{ex}} \end{aligned} \quad (7a)$$

with the abbreviation $b_\rho = \langle \omega_\rho^2 \rangle / 4\omega_{\text{eff}}^2 \Gamma_v$. According to Eq. (7a) the concentration c_v^{ex} of the excess vacancies can easily be obtained from the experimental data by subtracting the contribution $1/T_{1\rho}|_{\text{Diff}}^0 = A(\omega_1) b_\rho c_v$ in knowledge of b_ρ , i.e., of the vacancy jump rate Γ_v . One has to take into account, however, that besides the diffusion-induced contribution, $1/T_{1\rho}|_{\text{Diff}}$, a further relaxation rate process $1/T_{1\rho}|_{\text{ce}}$ is significant in metals such as aluminum which is caused by conduction-electron fluctuations at the sites of the nuclear probes via Fermi-contact interaction. This contribution varies linearly with temperature, and can be expressed as^{17,19}

$$\frac{1}{T_{1\rho}} \Big|_{\text{ce}} = A(\omega_1) CT . \quad (8)$$

Hence, the total NSR rate $1/T_{1\rho}$ measured in the experiments has to be written in terms of two contributions:

$$\frac{1}{T_{1\rho}} = A(\omega_1) CT + \frac{1}{T_{1\rho}} \Big|_{\text{Diff}} . \quad (9)$$

III. EXPERIMENTAL DETAILS

Ultrapure (5N) polycrystalline aluminum with a grain size of the order of 100 μm was used in the investigation. To avoid skin-effect distortion of the NMR signal, the actual NMR experiment was carried out on a single rectangular foil of size 27 mm \times 12 mm \times 25 μm . In the NMR experiments the sample under investigation is plastically deformed at a constant strain rate $\dot{\epsilon}$ by a servohydraulic tensile machine developed for temperature-variable NMR experiments.²⁰ During the deformation of the specimen, Al NSR rates $1/T_{1\rho}$ are measured in a fixed time interval Δt at raising times t_i , correspond to increasing average strains

$$\langle \varepsilon_i \rangle = \varepsilon_i(t_i) + \Delta t / 2 \cdot \dot{\varepsilon} .$$

Before and after each experimental run, the background contribution was measured by setting $\dot{\varepsilon} = 0$. The actual temperature was controlled by a thermocouple within an accuracy of about 1 K.

In order to increase the accuracy of the experiment we have improved the usual spin-locking technique used for $T_{1\rho}$ measurements. The traditional $T_{1\rho}$ technique consists of a short $\pi/2$ pulse which turns the nuclear magnetization into the y direction of the rotating frame perpendicular to the applied magnetic field B_0 . The pulse is followed by an rf field of strength B_1 and period t shifted in phase by 90° with respect to the $\pi/2$ pulse, i.e., the B_1 field (locking field) is aligned with the nuclear magnetization. The magnetization relaxes in the locked state with the relaxation time $T_{1\rho}$ according to

$$M_\rho(t) = M_\rho(0) \exp(-t/T_{1\rho}) , \quad (10)$$

where

$$M_\rho(0) = \frac{\omega_1^2}{\omega_1^2 + \omega_{loc}^2} . \quad (10a)$$

The actual value of $M_\rho(t)$ is measured by recording the height of the free induction decay $F(t)$ at $t = \tau$; i.e., $M_\rho(\tau) \equiv F(\tau)$. In order to measure $M_\rho(t)$ at different times one has to repeat the experiment varying the period τ of the locking field.

As depicted in the inset of Fig. 1, in the present CUT sequence method the locking field is cut into a large number n of pulses of duration t_p separated by short "observation window" of length t_w (i.e., $t_w \ll t_p$). Furthermore, the duration of t_w has to fulfill the condition $t_w \ll T_2$, where T_2 includes all inhomogeneous line broadening mechanisms. A single-shot experiment thus provides n values of the decay function of $M_\rho(t)$. It should be noted at this point that such pulse se-

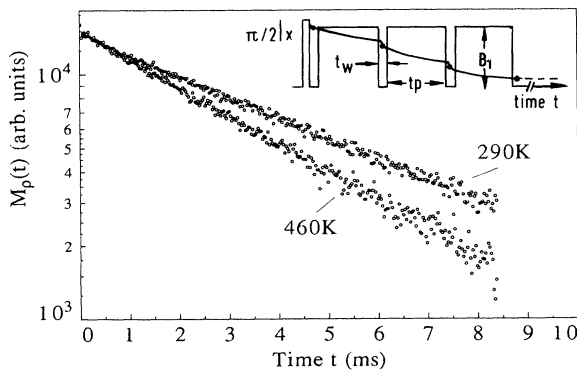


FIG. 1. Single-shot measurement of the Al nuclear magnetization decay in the rotating frame $M_\rho(t)$ in aluminum for two different temperatures. Inset: CUT sequence used for the measurements with $t_p = 20 \mu\text{s}$, $t_w = 8 \mu\text{s}$, $B_1 = 4.5 \text{ G}$.

quences were discussed in the past by several investigators. Ostroff and Waugh²¹ were the first to have demonstrated that the nuclear magnetization can be spin locked by a train of pulses. In their case the pulse train was preceded by an initial $\pi/2$ pulse whose phase was shifted by 90° relative to that of the pulse train. The time constant of the nuclear magnetization decay was shown to approach $T_{1\rho}$ in the limit of zero separation between pulses in the train. Rhim, Burum, and Elleman^{22,23} have analyzed theoretically the Ostroff-Waugh sequence showing that the spin-temperature assumption can be applied to explain the long-term (i.e., $T_{1\rho}$) behavior of the spin system. Others have applied similar approaches to the study of slow motions of OH^- in zeolites²⁴ and of protons in p-methoxybenzylidene-p-n-butylaniline (MBBA).²⁵

We found experimentally that the time constant of the decay agrees exactly with the expected relaxation time $T_{1\rho}$ in the rotating frame if the duration t_p of the locking pulses is given by the condition $t_p = \pi/4\gamma B_1$. Hence

$$M_\rho[n(t_p + t_w)] = M_\rho(0) \exp\left[-\frac{n(t_p + t_w)}{T_{1\rho}}\right] . \quad (10b)$$

The strength of the applied locking field B_1^{ext} is reduced by the relative width of the pulses, i.e., $B_1 = B_1^{\text{ext}} t_p / (t_p + t_w)$ for $t_w \ll t_p$. Otherwise the dependence of B_1 on the parameters t_p and t_w is more complicated because spectral components other than the Rabi frequency contribute to the spectral density.

Figure 1 shows an example of the time evolution of $M_\rho(t)$ of Al in aluminum measured with the CUT sequence at two different temperatures under an operating frequency of 41 MHz corresponding to a field strength of $B_0 = 3.7 \text{ T}$ for $\dot{\varepsilon} = 0$. The parameters of the sequence were $t_p = 20 \mu\text{s}$, $t_w = 8 \mu\text{s}$, and $B_1 = 4.5 \text{ G}$. As can be seen from Fig. 1 the new technique makes it feasible to obtain the entire time evolution of the magnetization M_ρ eliminating uncertainties concerning the initial magnetization $M_\rho(0)$ and the exponentiality of the decay of $M_\rho(t)$.

As depicted in Fig. 2 it is possible to demonstrate by the CUT sequence the strong effect of a small deviation ν_{off} of the operating frequency ν from the Larmor frequency ν_0 ($\nu_{\text{off}} = \nu - \nu_0$) on the decay of the nuclear magnetization. Obviously, a very small deviation ν_{off}/ν_0 of the order of 10^{-5} leads to a remarkable error in the determination of the relaxation rate. Mathematically, the decay function under off-resonance condition is given by

$$M_\rho(t) = M_\rho(0) \left[\left[1 - \frac{\nu_{\text{off}}}{\nu_1} \frac{T_{1\rho}}{T_1} \right] \exp\left[-\frac{t}{T_{1\rho}}\right] + \frac{\nu_{\text{off}}}{\nu_1} \frac{T_{1\rho}}{T_1} \right] , \quad (11)$$

where $\nu_1 = \omega_1/2\pi$ and T_1 denotes the Zeeman spin-lattice relaxation time.

In order to prove that the CUT sequence leads to the same results as the traditional $T_{1\rho}$ sequence, we have repeated the Al NSR measurements on pure aluminum as carried out by Fradin and Rowland.²⁶ The result is

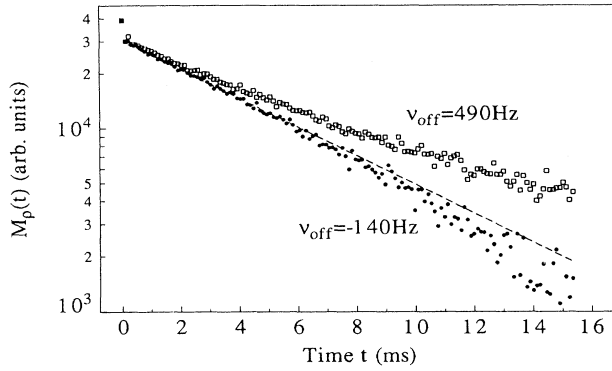


FIG. 2. Off-resonance decay of the Al nuclear magnetization $M_\rho(t)$ in aluminum for two different off-resonance frequencies $\nu_{\text{off}} = (\nu - \nu_0)/\nu_0$. Dashed line: on-resonance decay. The deviation from an exponential leads to a remarkable error in the determination of the NSR rate $T_{1\rho}$.

shown in Fig. 3. As predicted by Eq. (9) the observed NSR rate $1/T_{1\rho}$ consists of a conduction-electron contribution and a diffusion-induced contribution which becomes dominant above 550 K. The solid lines are fits to the data by means of Eqs. (1), (2), (4), (6), and (9) using the best-fit parameters listed in Table I [see Eqs. (2) and (4)]. The observed activation energy is in excellent accord with those obtained by Fradin and Rowland.²⁶ For the investigation presented in the next section it is important to note that the relaxation rate maximum of $1/T_{1\rho}$ occurs at about 630 K, i.e., Eq. (7) is valid for Al in aluminum below about 600 K. Furthermore, Fig. 3 also exhibits the temperature variation of the Zeeman NSR rate $1/T_1$ which is controlled by the conduction-electron mechanism in the entire temperature region [Eq. (8)].

IV. NMR EXPERIMENTS UNDER DEFORMATION

Mechanical deformation at a strain rate $\dot{\epsilon}$ leads to a change of the evolution of the nuclear magnetization, i.e.,

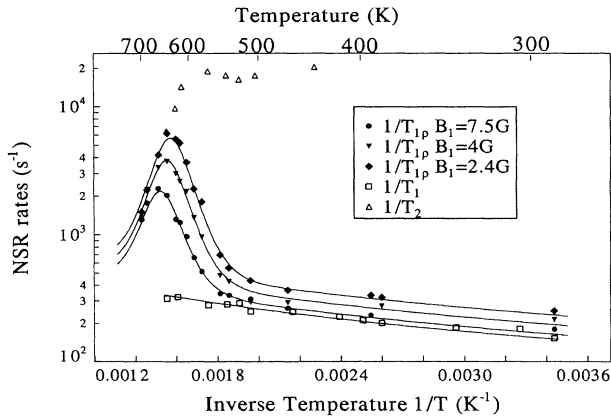


FIG. 3. Arrhenius plots of Al rates of Zeeman spin-lattice relaxation ($1/T_1$), spin-spin relaxation ($1/T_2$), and spin-lattice relaxation in the rotating frame ($1/T_{1\rho}$) for different locking fields B_1 using the CUT sequence in 5N aluminum. Solid lines are fits to the data by Eqs. (1), (2), (4), (6), and (9) with the fit parameters listed in Table I.

TABLE I. Summary of the parameters used for the ^{27}Al NMR measurements shown in Fig. 3.

$H_m + H_F$	1.27 eV
$\Gamma_0 \exp(S_f/k)$	4.65×10^{14} s
$\langle \omega_\rho^2 \rangle$	2.58×10^8 s $^{-2}$
ω_{loc}^2	2.18×10^8 s $^{-2}$
C	0.5 s $^{-2}$
δ	2

to a variation of the NSR rate $1/T_{1\rho}$. An example is depicted in Fig. 4 for Al in aluminum before ($\dot{\epsilon}=0$) and during ($\dot{\epsilon}=0.9$ s $^{-1}$) deformation measured at $T=300$ K. In order to determine correctly the contribution $1/T_{1\rho}^{\text{ex}}$ [see Eq. 7(a)] from the data one has to take into account that the deformation process does not only generate excess vacancies but also creates additional dislocations. The related strain ϵ gives rise to an increase of the quadrupolar part ω_Q of the local field ω_{loc} [see Eq. (6a)]. We found experimentally $\omega_{\text{loc}}^2 = \omega_{\text{loc}}^2(0) + A \cdot \epsilon$, where $\omega_{\text{loc}}^2(0) = 2.2 \times 10^8$ s $^{-2}$ and $A = 6.9 \times 10^9$ s $^{-2}$ with A being independent of strain rate and temperature in the temperature range under investigation. The latter is supported by measurements of the temperature dependence of the critical shear stress in aluminum.²⁷ Between 200 and 600 K the flow stress is found to be independent of temperature.

As depicted in Fig. 4 the strain dependence of the local field is responsible for two effects: Firstly, according to Eq. (10a) the strain creates an offset $\Delta M_\rho(0)$ of the magnetization. Secondly, as the strain increases linearly with time at a constant strain rate, the coefficient $A(\omega_1)$ in Eqs. (6) and (9) varies slightly with time resulting in a weak increase of the slope of the “background” magnetization decay compared to the slope of the decay for $\dot{\epsilon}=0$. The total background decay during the deformation process is indicated by the dashed line in Fig. 4. The actual value of $1/T_{1\rho}^{\text{ex}}$ results from the difference of the slopes of the decay measured under the strain rate of

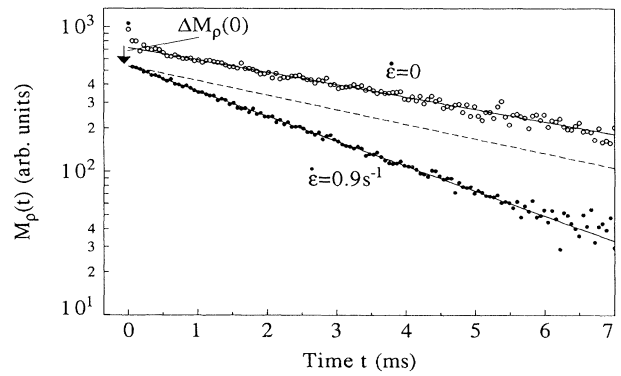


FIG. 4. Al nuclear magnetization decay $M_\rho(t)$ in 5N aluminum without ($\dot{\epsilon}=0$) and under ($\dot{\epsilon}=0.9$ s $^{-1}$) deformation at 300 K. Dashed line: Effective background decay during deformation (see text). The excess vacancy contribution to the decay, i.e., $1/T_{1\rho}^{\text{ex}}$ is obtained from the difference between the decay for $\dot{\epsilon}=0.9$ s $^{-1}$ and the background decay.

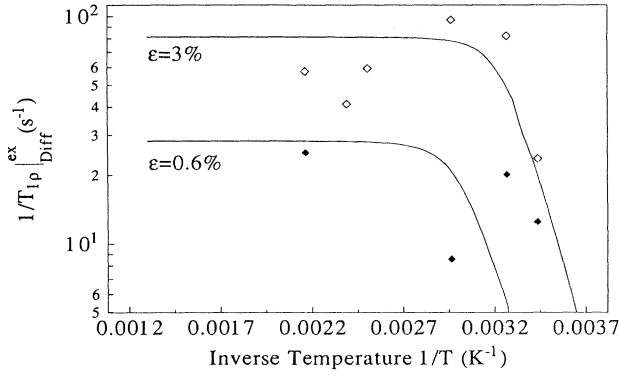


FIG. 5. Temperature dependence of the excess vacancy contribution to the Al NSR rate, $1/T_{1\rho}|_{Diff}^{ex}$, in aluminum at $\dot{\epsilon}=0.55$ s^{-1} for two different strains. Solid lines are fits to the data by means of model (1). Note that the NSR rates become temperature independent at elevated temperatures as predicted by the model.

$\dot{\epsilon}=0.9$ s^{-1} and the total background decay (dashed line).

By means of the CUT sequence and the evaluation procedure discussed above we have measured the diffusion-induced excess relaxation rate, $1/T_{1\rho}|_{Diff}^{ex}$, of Al on deforming aluminum as a function of temperature, strain rate, and average strain. Results of such measurements are presented in Figs. 5 and 6. In Fig. 5, the temperature dependence of $1/T_{1\rho}|_{Diff}^{ex}$ is exhibited for two different strains using a strain rate $\dot{\epsilon}=0.55$ s^{-1} . Figure 5 demonstrates clearly, that $1/T_{1\rho}|_{Diff}^{ex}$, and therefore the concentration of the excess vacancies depends on strain, and vanishes for elevated temperatures because of a rising annihilation rate due to an increase of the vacancy diffusion (see Sec. VI). The solid lines are fits to the data based on a model presented in the next section. Figure 6 shows a contour plot of $1/T_{1\rho}|_{Diff}^{ex}$ illustrating the dependence of the applied strain and strain rate of the excess NSR rate for two different temperatures. The contour net in Fig. 6 represents a fit to the data.

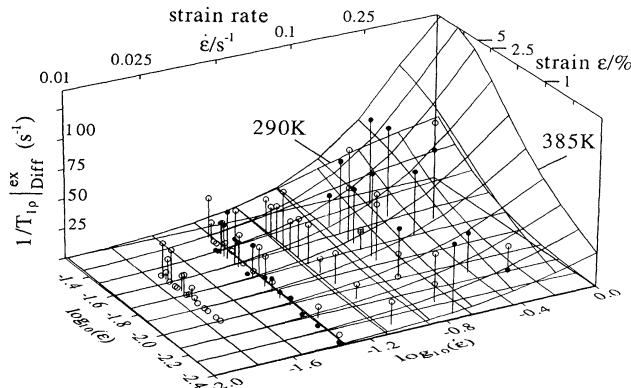


FIG. 6. Al NSR rate contribution $1/T_{1\rho}|_{Diff}^{ex}$ in aluminum as a function of strain ϵ and strain rate $\dot{\epsilon}$ for two different temperatures. The marked contour net is a best-fit to the data using model (1).

V. STRAIN-INDUCED VACANCIES

Plastic deformation of a crystalline solid is known to create an additional number of vacancies due to the intersection of screw dislocations which annihilate simultaneously through migration to sinks. The concentration c_v^{ex} of these vacancies obeys the rate equation²⁸

$$\dot{c}_v^{ex} = \dot{c}_v^{ex}|_f + \dot{c}_v^{ex}|_a, \quad (12)$$

where the subscripts f and a indicate the formation and annihilation, respectively. The formation process is governed by the nonconservative motion of jogs on screw dislocations under a strain rate $\dot{\epsilon}$:²⁹

$$\dot{c}_v^{ex}|_f = \alpha(T, \rho(\epsilon))\dot{\epsilon}, \quad (13)$$

where $\rho(\epsilon)$ denotes the strain-dependent dislocation density. Different approaches have been developed in the literature concerning the coefficient α depending on the mechanism of the jog production. Mecking and Estrin³⁰ assume that the jogs with formation energy $E_j \approx 0.1Gb^3$ (G is the shear modulus, b is the Burgers vector) are produced mechanically by the applied work. Then, α becomes independent of temperature and is proportional to the applied stress and inversely proportional to the formation energy E_j . The corresponding vacancy formation rate is given by³⁰

$$\dot{c}_v^{ex}|_f^{(1)} = \chi \frac{\sigma}{E_j} \dot{\epsilon}, \quad (14)$$

where χ denotes the fraction of the applied mechanical power density $\sigma\dot{\epsilon}$ used for vacancy formation via jog production. Using the relation $\sigma = k_1\sqrt{\rho}$, Eq. (14) can be rewritten as

$$\dot{c}_v^{ex}|_f^{(1)} = k_1 \chi \frac{\sqrt{\rho(\epsilon)}}{E_j} \dot{\epsilon}. \quad (14a)$$

A similar approach for the coefficient α is suggested by Lenasson.³¹ In his model, the jogs are generated by intersections between the moving and the forest dislocations. Using the Orowan equation³² in which the strain rate $\dot{\epsilon}$ is related to the density and velocity of the mobile dislocations, the vacancy formation rate is proportional to the dislocation density

$$\dot{c}_v^{ex}|_f^{(2)} = k_2 \rho(\epsilon) \dot{\epsilon}. \quad (15)$$

If, on the other hand, one considers thermally produced jogs, one has for $\dot{c}_v^{ex}|_f$ (Ref. 13)

$$\dot{c}_v^{ex}|_f^{(3)} = \alpha_0(\epsilon) \exp\left[-\frac{E_j}{kT}\right] \dot{\epsilon}. \quad (16)$$

Though the various models differ with regard to the deformation-induced generation of vacancies they have in common that the vacancies disappear via diffusive motion to dislocations acting as primary vacancy sinks.

Following Mecking and Estrin³⁰ we exclude the recombination of the excess vacancies with interstitials. This assumption is confirmed by Mössbauer experiments on cold-worked aluminum.³ The annihilation rate can be written then as³⁰

$$\dot{c}_v^{\text{ex}}|_a = -\beta_0 \frac{\Gamma_v(T)}{\lambda^2(\varepsilon)} c_v^{\text{ex}}, \quad (17)$$

where $\Gamma_v = \Gamma_{v0} \exp(-E_m/kT)$ denotes the thermally activated jump rate of the vacancies with E_m being the migration energy, λ is the mean distance between the sinks, and β_0 is a coefficient independent of the test conditions. For a random distribution of dislocations one has $\lambda^2 \approx 1/\rho(\varepsilon)$, while a cell structure of the dislocations with diameter d yields $\lambda \approx d$ approximately independent of strain ε . In the present discussion we have assumed a random distribution of dislocations. Furthermore, we do not distinguish explicitly between screw and edge dislocations.

In order to solve Eq. (12) for one of the models one has to relate the actual strain ε with the corresponding dislocation density ρ . Here we follow the one-parameter approach of Kocks:³³

$$\frac{d\rho}{d\varepsilon} = a\sqrt{\rho} - c_1(\dot{\varepsilon}, T)\rho \quad (18)$$

saying that the dislocations are formed by the applied stress σ using $\sigma \propto \sqrt{\rho}$ and disappear through a kinetic reaction of first order. The solution of Eq. (7) can be written as

$$\rho(\varepsilon) = \rho_{\text{eq}} \left[1 - \frac{\sqrt{\rho_{\text{eq}}} - \sqrt{\rho_0}}{\sqrt{\rho_{\text{eq}}}} \exp\left[-\frac{1}{2}c_1\varepsilon\right] \right]^2, \quad (19)$$

where $\rho_{\text{eq}} \equiv a^2/c_1^2$ and ρ_0 denotes the initial dislocation density at $\varepsilon=0$. Contrary to the coefficient a , the annihilation coefficient c_1 depends in general on strain rate and temperature. As discussed in Sec. IV, however, c_1 can be supposed to be constant for aluminum in the temperature range between 200 and 600 K. Figure 7 presents a graph of the solution [Eq. (18)] using $\rho_0 = 1 \times 10^{11} \text{ m}^{-2}$ and $\rho_{\text{eq}} = 3.4 \times 10^{16} \text{ m}^{-2}$. For small strains, ρ increases linear-

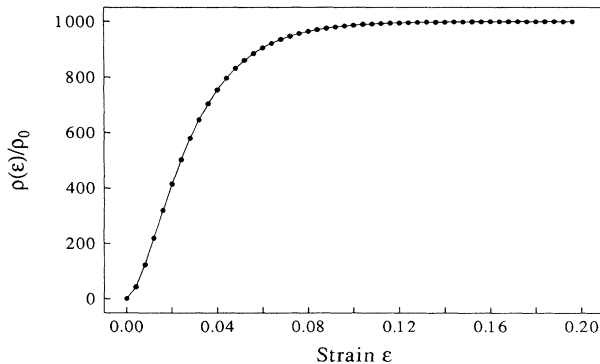


FIG. 7. Strain dependence of the relative dislocation density $\rho(\varepsilon)/\rho_0$ according to Eq. (19).

ly with rising strain, while for large strains the dislocation density approaches the equilibrium value ρ_{eq} .

Mostly, the steady-state condition $\dot{c}_v^{\text{ex}}=0$ is introduced [Eq. (12)] in order to calculate expressions for the strain-induced concentration of the excess vacancies. However, our experimental findings reveal that one has to solve Eq. (12) under a nonsteady state condition, i.e., $\dot{c}_v^{\text{ex}} \neq 0$ in order to interpret the data correctly.

In the following figures the solutions obtained by numerical calculations are depicted for the three models introduced at the beginning of this section. Furthermore, approximate relations of the excess vacancy concentration c_v^{ex} are presented which are valid for low and high temperatures. The calculations are performed for aluminum using $\Gamma_v(T) = 2 \times 10^{14} \exp(-0.62 \text{ eV}/kT) \text{ s}^{-1}$, $E_j = 0.4 \text{ eV}$, $c_1 = 86$, $\chi = 1.3 \times 10^{-27} \text{ m}^3$, $\rho_{\text{eq}} = 3.4 \times 10^{16} \text{ m}^{-2}$.

A. Model (1): Eqs. (12), (14a), (17), and (19)

Solutions of the rate Eq. (12) are performed by Eqs. (14a), (17), and (19) using the conditions $\rho_{\text{eq}} \gg \rho_0$, $4 \ll c_1 \varepsilon \exp(0.5c_1\varepsilon) + \exp(-0.5c_1\varepsilon)$, and are presented in Fig. 8 for two different strains ($\varepsilon = 2\%$ and 20%). The figure exhibits the dependence of the excess vacancy concentration on temperature and strain rate. Obviously, one can distinguish two different temperature regions: Above a transition temperature T^* , c_v^{ex} is thermally activated and increases linearly with rising strain rate depending slightly on strain. The high-temperature approximation can be expressed as

$$c_v^{\text{ex}}|_{\text{high } T} = A_h^{(1)} \chi \frac{1}{\sqrt{\rho_{\text{eq}}}} \left[1 - \exp\left[-\frac{b}{2}\varepsilon\right] \right] \times \exp\left[\frac{E_m}{kT}\right] \dot{\varepsilon} \quad (20a)$$

with $A_h^{(1)}$ being a constant.

Below T^* , c_v^{ex} becomes independent of strain rate and temperature, but increases linearly with increasing strain.

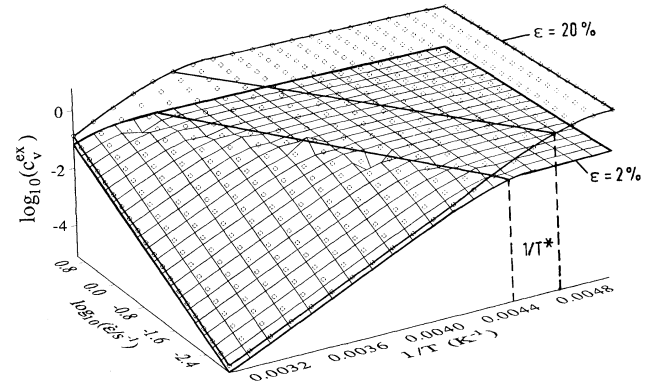


FIG. 8. Excess vacancy concentration c_v^{ex} as a function of strain and inverse temperature for two different strains (2%, 20%) as calculated from model (1). Note the two temperature regions [see Eqs. (20a) and (20b)] separated by the transition temperature T^* [Eq. (21)].

The corresponding solution is given by

$$c_v^{\text{ex}}|_{\text{low}T} = A_l^{(1)} \chi \sqrt{\rho_{\text{eq}} \epsilon} . \quad (20b)$$

The transition temperature T^* depends logarithmically on strain and strain rate

$$T^* = \frac{E_m}{k} \frac{1}{\ln(a_1 \Gamma_{v0} \epsilon / \dot{\epsilon})} \quad (21)$$

with $a_1 = \beta_0 \rho_{\text{eq}}$.

B. Model (2): Eqs. (12), (15), (17), and (19)

As suggested by the similarity between Eq. (14a) and Eq. (15) the excess vacancy concentration c_v^{ex} resulting from model (2) is like that of model (1). This is illustrated by the graphics of the solution of model (2) for two different strains presented in Fig. 9. Again, one obtains a high-temperature approximation where the vacancy concentration c_v^{ex} depends Arrhenius-like on temperature and is proportional to the strain rate

$$c_v^{\text{ex}}|_{\text{high}T} = A_h^{(2)} \exp \left[\frac{E_m}{kT} \right] \dot{\epsilon} , \quad (22a)$$

and a solution for low temperatures where the vacancy concentration varies linearly with strain

$$c_v^{\text{ex}}|_{\text{low}T} = A_l^{(2)} \rho_{\text{eq}} \epsilon . \quad (22b)$$

($A_h^{(2)}$, $A_l^{(2)}$: constant coefficients). The main difference between the two models is the missing strain dependence of the high-temperature approximation (22a) compared to the corresponding relation (21a). As in model (1), the transition between the low-temperature and the high-temperature behavior occurs at a critical temperature T^* which depends on strain and strain rate according to Eq. (21).

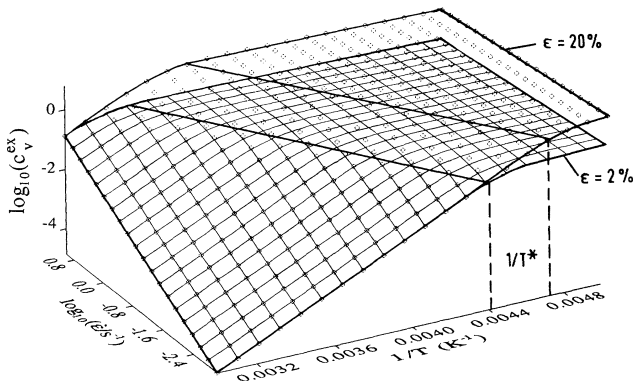


FIG. 9 Same as in Fig. 8 calculated from model (2). Solutions look very similar to the solutions shown in Fig. 8 because of the similarity of the two approximations [see Eqs. (21a) and (21b)].

C. Model (3): Eqs. (12), (16), (17), and (19)

In contrast to models (1) and (2) the formation process of the excess vacancies in model (3) is supposed to be thermally activated [see Eq. (16)]. The assumption results in an Arrhenius-like temperature dependence of the excess vacancy concentration for both low and high temperatures. The corresponding approximations are

$$c_v^{\text{ex}}|_{\text{high}T} = A_h^{(3)} \exp \left[\frac{E_m - E_j}{kT} \right] \dot{\epsilon} , \quad (23a)$$

$$c_v^{\text{ex}}|_{\text{low}T} = A_l^{(3)} \exp \left[-\frac{E_j}{kT} \right] \dot{\epsilon} \quad (23b)$$

with $A_h^{(3)}$ and $A_l^{(3)}$ being constant coefficients. The complete solutions of model (3) are presented in Fig. 10 for two different strains. The figure illustrates the temperature regimes where either the approximation (23a) and or (23b) is relevant. As in models (1) and (2) the transition temperature T^* separating the two regions depends on strain and strain rate according to Eq. (21).

In conclusion one should note that the solutions [(20a), (20b), (22a), (22b), (23a), and (23b)] do answer a long-standing question as to whether the concentration of strain-induced vacancies is proportional to strain or to strain rate. Independent of the model, both answers are correct depending on the actual experimental conditions such as strain, strain rate, and temperature.

VI. EVALUATION AND DISCUSSION

The concentration c_v^{ex} of the excess vacancies in deforming aluminum was determined from the experimental data displayed in Figs. 5 and 6 by means of the relation $1/T_{1\rho}^{\text{ex}}|_{\text{Diff}} = A(\omega_1) b_\rho c_v^{\text{ex}}$ given in Eq. (7a). Trying to compare the findings with the models presented in Sec. V we found that model (1) agrees best with the data. The complete solution of the corresponding rate equation can be expressed as

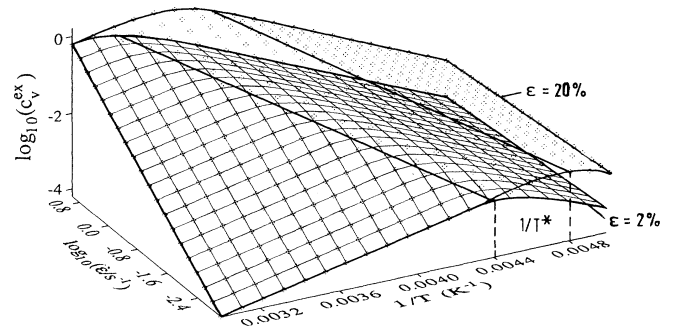


FIG. 10. Same as in Fig. 8 calculated from model (3). Contrary to models [(1) and (2)] the model (3) leads to a temperature dependence of c_v^{ex} also below the transition temperature T^* [see Eqs. (23a) and (23b)].

$$c_v^{\text{ex}} = c_{v,\text{eq}}^{\text{ex}} \left[1 - \exp \left[-\beta_0 \rho_{\text{eq}} \Gamma_v \frac{\varepsilon}{\dot{\varepsilon}} \right] (1 - c_2) - c_2 \exp \left[-\frac{c_1}{2} \varepsilon \right] \right], \quad (24)$$

where

$$c_{v,\text{eq}}^{\text{ex}} = \frac{k_1 \chi}{E_j \sqrt{\rho_{\text{eq}} \beta_0} \Gamma_v} \dot{\varepsilon} \quad (24a)$$

and

$$c_2 = \frac{1}{1 - (c_1/2\beta_0\rho_{\text{eq}}\Gamma_v)\dot{\varepsilon}}. \quad (24b)$$

A best fit to the data by means of Eq. (24) is illustrated by the solid lines in Fig. 5 and in particular by the contour net in Fig. 6 using the following set of parameters: $\rho_{\text{eq}} \equiv a^2/c_1^2 = 3.4 \times 10^{16} \text{ m}^{-2}$, $\beta_0 = 8.3 \times 10^{-20} \text{ m}^2$, $k_1 = 0.33Gb$, $G = 2.8 \times 10^4 \text{ MPa}$, $b = 0.286 \text{ nm}$, $k_1\chi/E_j = 5.4 \times 10^{-8}$. Inserting the parameters yields the following relation for the vacancy concentration:

$$c_v^{\text{ex}} = 3.6 \times 10^3 \frac{\dot{\varepsilon}}{\Gamma_v} \left[1 - \exp \left[-0.003 \Gamma_v \frac{\varepsilon}{\dot{\varepsilon}} \right] (1 - c_2) - c_2 \exp(-43\varepsilon) \right] \quad (25)$$

with $c_2 = 1/(1 - 15301\dot{\varepsilon}/\Gamma_v)$ and

$$\Gamma_v = 2 \times 10^{14} \exp(-0.62 \text{ eV}/kT) \text{ s}^{-1}.$$

It should be noted that the approximation presented here diverges at the critical temperature T^* , i.e., $c_2 \rightarrow \infty$ if the actual strain ε reaches the value $2/c_1$.

As expected the high-temperature approximation of Eq. (25) which is determined by the condition $0.003\Gamma_v\varepsilon/\dot{\varepsilon} \gg 1$ is in agreement with Eq. (20a):

$$c_v^{\text{ex}}|_{\text{high}T} = 3.6 \times 10^3 / \Gamma_v [1 - c_2 \exp(-43\varepsilon)]. \quad (25a)$$

It is interesting to remark that the related NSR rate contribution $1/T_{1\rho}^{\text{ex}}|_{\text{Diff}}$ does not depend on temperature as confirmed by the data (see Fig. 5). The reason is an elimination of the jump rate Γ_v in the expression for $1/T_{1\rho}^{\text{ex}}|_{\text{Diff}}$: Inserting Eq. (25a) into Eq. (7a) yields $1/T_{1\rho}^{\text{ex}}|_{\text{Diff}} \propto c_v^{\text{ex}}/\Gamma_v \propto \text{const}\Gamma_v/\Gamma_v = \text{const}$.

The corresponding approximation of Eq. (25) at low temperatures ($0.003\Gamma_v\varepsilon/\dot{\varepsilon} \ll 1$) can be expressed as

$$c_v^{\text{ex}}|_{\text{low}T} \approx 9.7\varepsilon, \quad (25b)$$

which corresponds to the relation (20b). Furthermore, the analysis of the data yields a value $1.3 \times 10^{-27} \text{ m}^3$ for the coefficient χ in Eq. (14). Assuming a typical activation volume $\lambda^3 \approx \rho_{\text{eq}}^{-3/2} \approx 1.6 \times 10^{-25} \text{ m}^3$ one obtains an efficiency $\chi' = \chi/\lambda^3 \approx 1\%$ for the conversion of the applied mechanical work into excess vacancies.

In order to illustrate the results of the analysis present-

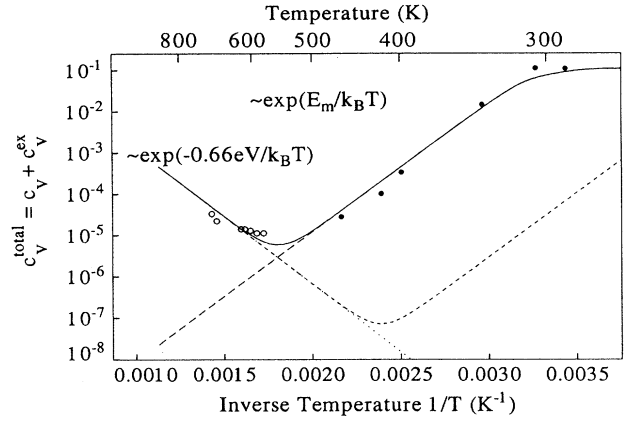


FIG. 11. Temperature variation of the total vacancy concentration $c_v^{\text{total}} = c_v + c_v^{\text{ex}}$ in pure aluminum under deformation. The intrinsic vacancies c_v are significant above 550 and 400 K, respectively [$\varepsilon = 2.7\%$; $\dot{\varepsilon} = 0.55 \text{ s}^{-1}$ (solid line), $\dot{\varepsilon} = 10^{-4} \text{ s}^{-1}$ (dashed line)], while below these temperatures the excess vacancies become dominant [see Eq. (20a)].

ed by Eq. (25) the temperature variation of the total vacancy concentration $c_v^{\text{total}} = c_v + c_v^{\text{ex}}$ in aluminum is plotted in Fig. 11 using $c_v = 23 \exp(-0.66 \text{ eV}/kT)$ as obtained by Seeger, Wolf, and Mehrer³⁴ and the deformation parameters $\varepsilon = 2.7\%$ and $\dot{\varepsilon} = 0.55 \text{ s}^{-1}$ and 10^{-4} s^{-1} , respectively, used in the actual experiment. The data points obtained by the experiments are depicted, too. The figure shows that, for $\dot{\varepsilon} = 0.55 \text{ s}^{-1}$, above about 550 K the thermally created vacancies are dominant whereas below 550 K the strain-induced vacancy contribution becomes significant as it rises exponentially with decreasing temperature according to Eq. (25a). Below the transition temperature $T^* \approx 240 \text{ K}$, however, the vacancy concentration levels off, i.e., the transition from the high-temperature approximation (25a) to the low-temperature approximation (25b) occurs. Here, the excess vacancy concentration is controlled only by the actual strain ε .

In summary the present investigation shows that an *in situ* observation of excess vacancies under plastic deformation can be performed in metals. The actual concentration of the excess vacancies was obtained by an improved NMR technique (CUT sequence) in order to carry out a fast registration of the decay of the nuclear magnetization in the rotating frame. The experimental results were found to agree best with model (1) where a fraction of about 1% of the applied mechanical work is spent for the vacancy production, and the vacancies annihilate via migration to dislocations acting as sinks.

ACKNOWLEDGMENTS

We thank Professor T. Hehenkamp for useful discussions. The work was financially supported by the Deutsche Forschungsgemeinschaft (DFG) and the Foundation for Fundamental Research on Matter (FOM). We acknowledge the travel grants provided by the State Government of Nordrhein-Westfalen and of North Carolina.

- ¹H. Murakami and S. Yoshida, *Cryst. Lattice Defects* **6**, 89 (1975).
- ²W. Kohl, R. Scheffel, H. Heidsiek, and K. Lücke, *Acta Metall.* **31**, 1895 (1983).
- ³A. Sen Gupta and R. Roy, *Solid State Commun.* **75**, 843 (1990).
- ⁴J. A. Jackman, G. M. Hood, and R. J. Schultz, *J. Phys. F.* **17**, 1817 (1987).
- ⁵B. Wodniecka, M. Marszalek, and P. Wodniecki, *J. Phys. Condens. Matter* **1**, 7521 (1989).
- ⁶G. Guenin, J. Perez, and P. F. Gobin, *Cryst. Lattice Defects* **3**, 199 (1972).
- ⁷K. Sassa, W. Petry, and G. Vogl, *Philos. Mag. A* **48**, 1 (1983).
- ⁸C. Kisielowski-Kemmerich, J. Czaschke, and H. Alexander, *Mater. Sci. Forum* **10-12**, 745 (1986).
- ⁹Z. Gyulai and D. Hartley, *Z. Phys.* **51**, 378 (1928).
- ¹⁰M. Ueta and W. Känzig, *Phys. Rev.* **94**, 1390 (1954); **97**, 1951 (1955).
- ¹¹F. S. Buffington and M. Cohen, *Trans. AIME* **194**, 859 (1952).
- ¹²A. R. Wazzan and J. E. Dorn, *J. Appl. Phys.* **36**, 222 (1965).
- ¹³K. Detemple, O. Kanert, K. L. Murty, and J. Th. M. De Hosson, *Phys. Rev. B* **44**, 1988 (1991).
- ¹⁴H. Mehrer, *J. Nucl. Mater.* **69**, 38 (1978).
- ¹⁵A. R. Allnat and A. B. Lidiard, *Atomic Transport in Solids* (Cambridge University Press, Cambridge, 1993).
- ¹⁶O. Kanert, *Phys. Rep.* **91**, 185 (1982).
- ¹⁷D. Wolf, *Spin-temperature and Nuclear-Spin Relaxation in Matter* (Clarendon, Oxford, 1979).
- ¹⁸H. C. Torrey, *Phys. Rev.* **92**, 962 (1953).
- ¹⁹J. Korringa, *Physica* **16**, 601 (1950).
- ²⁰H. Hackeloer, O. Kanert, H. Tamler, and J. Th. M. De Hosson, *Rev. Sci. Instrum.* **54**, 341 (1983).
- ²¹E. D. Ostroff and J. S. Waugh, *Phys. Rev. Lett.* **16**, 1096 (1966).
- ²²W. K. Rhim, D. P. Burum, and D. D. Ellemann, *Phys. Rev. Lett.* **37**, 1764 (1976).
- ²³W. K. Rhim, D. P. Burum, and D. D. Ellemann, *J. Chem. Phys.* **68**, 692 (1978).
- ²⁴W. Gründer, H. Schmiedel, and D. Freude, *Ann. Phys.* **27**, 409 (1971).
- ²⁵L. R. Whalley and C. E. Tarr, *J. Magn. Reson.* **26**, 537 (1977).
- ²⁶F. Y. Fradin and T. J. Rowland, *Appl. Phys. Lett.* **11**, 207 (1967).
- ²⁷A. Seeger, *Moderne Probleme der Metallphysik* (Springer-Verlag, Berlin, 1965), Band 1.
- ²⁸P. G. McCormick and K. L. Murty, *Scr. Metall.* **6**, 225 (1972).
- ²⁹K. L. Murty, F. A. Mohammed, and J. E. Dorn, *Scr. Metall.* **5**, 1087 (1971).
- ³⁰H. Mecking and Y. Estrin, *Scr. Metall.* **14**, 815 (1980).
- ³¹C. G. Lenasson, *Scr. Metall.* **6**, 1125 (1972).
- ³²J. Friedel, *Dislocation* (Pergamon, New York, 1967).
- ³³U. F. Kocks, *J. Eng. Mater. Tech. (ASME-H)* **98**, 76 (1976).
- ³⁴A. Seeger, D. Wolf, and H. Mehrer, *Phys. Status Solidi B* **48**, 481 (1971).